AGU PUBLICATIONS

JGR

Journal of Geophysical Research: Space Physics

RESEARCH ARTICLE

10.1002/2015JA022025

Key Points:

- The Harang reversal is the solution of the steady plasma sheet convection for the interchange stability
- PVg increases/decreases along the convection flow for downward/upward FACs in a steady plasma sheet
- Auroral arcs in the premidnight R1/R2 currents mapped to the equator likely extend in the Sun-Earth/azimuthal direction

Correspondence to:
S. Ohtani,
ohtani@jhuapl.edu

Citation:
Ohtani, S., M. Gkioulidou, C.-P. Wang, and R. A. Wolf (2016), The Harang reversal and the interchange stability of the magnetotail, *J. Geophys. Res. Space Physics*, *121*, 3278–3292, doi:10.1002/2015JA022025.

Received 12 OCT 2015
Accepted 15 MAR 2016
Accepted article online 30 MAR 2016
Published online 30 APR 2016

The Harang reversal and the interchange stability of the magnetotail

Shinichi Ohtani[1], Matina Gkioulidou[1], Chih-Ping Wang[2], and Richard A. Wolf[3]

[1]The Johns Hopkins University Applied Physics Laboratory, Laurel, Maryland, USA, [2]Department of Atmospheric and Oceanic Sciences, University of California, Los Angeles, California, USA, [3]Department of Physics and Astronomy, William Marsh Rice University, Houston, Texas, USA

Abstract The present study addresses steady convection in the plasma sheet in terms of the interchange stability with special attention to the Harang reversal. The closure of the tail current with a field-aligned current (FAC) results from the divergence/convergence of the pressure gradient current. If the magnetotail is in a steady state, the associated change of local plasma pressure p has to balance with its advective change. Accordingly, for adiabatic transport, the flux tube entropy parameter pV^{γ} increases and decreases along the convection path in regions corresponding to downward and upward FACs, respectively. This requirement, along with the condition for the interchange stability imposes an important constraint on the direction of convection especially in the regions of downward FACs. It is deduced that for the dusk cell, the convection in the downward R2 current has to be directed azimuthally duskward, which follows the sunward, possibly dawnward deflected, convection in the region of the premidnight upward R1 current. This duskward turn of convection takes place in the vicinity of the R1-R2 demarcation, and it presumably corresponds to the Harang reversal. For the dawn cell the convection in the postmidnight downward R1 current has to deflect dawnward, and then it proceeds sunward in the upward R2 current. The continuity of the associated ionospheric currents consistently reproduces the assumed FAC distribution. The proposed interrelationships between the convection and FACs are also verified with a quasi-steady plasma sheet configuration and convection reproduced by a modified Rice Convection Model with force balance.

1. Introduction

Large-scale field-aligned currents (FACs) in the midnight-sector auroral oval are magnetically mapped to the plasma sheet, where perpendicular currents are driven primarily by the pressure gradient. Since in the plasma sheet the ion temperature is significantly higher than the electron temperature, the ions are the dominant contributor to the plasma pressure and therefore to the pressure gradient current, that is, the tail current. In contrast, the FACs are carried predominantly by electrons because of their high mobility along the magnetic field line. Where the tail current closes with a downward FAC (i.e., a FAC flowing toward the ionosphere), the pressure gradient current, and therefore, the ion number flux associated with the magnetic drift converges, and electrons move along the field line toward the region. That is, both ions and electrons accumulate. If we make a similar argument based on the energy flux, rather than the number flux, this means that the plasma pressure increases with time in the flux tube of a downward FAC; a more strict formulation is later described in section 2 and Appendix A. Where the tail current closes with an upward FAC (i.e., FACs flowing out of the ionosphere), in contrast, the continuous reduction of plasma pressure is expected.

This simple discussion, however, raises a fundamental question about the magnetotail dynamics, that is, how, or if, the magnetotail can be in a steady state. The plasma pressure is one of the most critical quantities for the stability of the magnetotail. More specifically, the interchange stability of the magnetotail can be addressed in terms of the spatial distribution of the flux tube entropy parameter, pV^{γ} [e.g., *Wolf et al.*, 2009]; p is plasma pressure, V is the flux volume per unit magnetic flux, and γ is the adiabatic index. If the plasma pressure p changes with time, so does pV^{γ}. Therefore, even if the magnetotail is interchange stable at one moment, it may not be so in the future. The issue is closely related to the pressure balance inconsistency [*Erickson and Wolf*, 1980], which is concerned with the enhancement of plasma pressure along the earthward convection in the plasma sheet. Although the steady state plasma transport from the plasma sheet to the ring current has been addressed numerically [*Hau*, 1991; *Lemon et al.*, 2004; *Wang et al.*, 2004], it still remains to understand how specifically the distributions of fundamental quantities such as convection, plasma pressure, and FACs are interrelated and what features result from the required self-consistency.

For the aforementioned issue about the change of pV^{γ} associated with the FAC closure, the convection must be the key. Although the FAC closure results from the divergence of the pressure gradient current and therefore from the divergence of the ion number flux associated with the magnetic drift, the ions also undergo the electric drift, that is, convection. It is along the total drift path, the path of the magnetic and electric drifts combined, that pV^{γ} is conserved if the transport is adiabatic; more precisely, the partial entropy of a specific energy invariant is conserved along the drift path of the corresponding element [*Wolf*, 1983]. If pV^{γ} locally remains constant, the change of pV^{γ} related to the FAC closure needs to be balanced by the advective change of pV^{γ} by convection. Therefore, if the magnetotail is in a steady state, the distributions of pV^{γ} and FACs have to be linked with the plasma sheet convection in such a way that the interchange stability of the magnetotail continues to hold.

The observation shows that the nightside FAC distribution consists of two current systems, that is, the R1 and R2 currents [*Iijima and Potemra*, 1976]. The R1 current flows out of and into the ionosphere in the premidnight and postmidnight sectors, respectively. The R2 current is located adjacently equatorward of the R1 current, and its polarity is the opposite of that of the R1 current in a given MLT sector. The FAC distribution is not symmetric with respect to midnight. Most noticeably, the premidnight upward R1 and postmidnight upward R2 currents are distributed continuously across midnight. In general, the nightside R1 current can be associated with the earthward convection in the plasma sheet, which may be regarded as the return flow of the global two-cell convection of the magnetosphere. In contrast, the R2 current is widely regarded as the manifestation of the shielding of the inner magnetosphere from this convection electric field. Thus, at least in the plasma sheet region corresponding to the R1 system, the X (Sun-Earth) component of the convection has to be primarily sunward. At the same time pV^{γ} decreases toward Earth [e.g., *Kaufmann et al*., 2004; *Xing and Wolf*, 2007; *Wang et al*., 2009]; in general, p increases with decreasing X distance in the plasma sheet, but V^{γ} decreases far more steeply so that pV^{γ} decreases sunward. Those basic features of the FACs, convection, and structure of the magnetotail should apply to the steady states of the plasma sheet.

In the present study we seek to address for the first time the plasma convection in the steady plasma sheet from the viewpoint of interchange stability. A convection structure of our particular interest is the Harang reversal [*Harang*, 1946], which in the ionosphere is characterized as the interface between the eastward and westward convection flows on its poleward and equatorward sides, respectively [*Heppner*, 1972; *Maynard*, 1974]. Whereas the original study by *Harang* [1946] was concerned with ground magnetic disturbances (i.e., equivalent currents), we define the Harang reversal in terms of convection. The associated latitudinal electric field converges at the reversal, suggesting that the reversal is collocated with an upward FAC; the distributions of convection and FACs are actually more complex because of the spatial gradient of ionospheric conductance (see section 4). We refer to this upward FAC as R1 current in this study following the convention although it is probably driven by the pressure gradient in the plasma sheet in the same way as the R2 current is driven (see section 3). Modeling studies also suggest that ion thermal kinetics play an essential role in the formation of the Harang reversal in the magnetosphere [*Erickson et al*., 1991; *Gkioulidou et al*., 2009; *Yang et al*., 2014].

The Harang reversal is often collocated with discrete auroral arcs, and substorm onsets very often take place in the vicinity of this reversal [e.g., *Bristow and Jensen*, 2007; *Weygand et al*., 2008; *Zou et al*., 2009a, 2009b]. Before substorm onsets the overall convection, currents, and aurora structures in the nightside ionosphere often change very gradually over prolonged ($>$1 h) periods [e.g., *Nielsen and Greenwald*, 1979; *Lessard et al*., 2007]. The convection in the plasma sheet, in contrast, is always bursty to some extent irrespective of geomagnetic activity [e.g., *Angelopoulos et al*., 1994], and numerous studies examined transient fast flows in the plasma sheet during the substorm growth phase. However, the occurrence of those flows is limited temporally and spatially, and the majority of them actually do not reach the near-Earth region [e.g., *Ohtani et al*., 2006; *Dubyagin et al*., 2011; *Kim et al*., 2012]. We therefore consider that during the substorm growth phase the magnetosphere-ionosphere (M-I) system in the near-Earth plasma sheet is quasi-steady at least from a global perspective, and it is an important application of this study. Another possible application is the steady magnetospheric convection events. The associated nightside ionospheric convection is also characterized by the Harang reversal [*Kissinger et al*., 2013], and in the plasma sheet fast flows are diverted either dawnward or duskward before reaching the near-Earth ($<$15 R_E) region [*Kissinger et al*., 2012].

The present paper is organized in the following way. In section 2 we formulate the change of pV^{γ} along the convection flow in the presence of the tail current closure with FACs. In section 3 we discuss the equatorial

distributions of p and V corresponding to the distribution of the R1 and R2 currents, and in section 4 we seek to reconstruct the quasi-steady convection in the plasma sheet based on the requirement for the interchange stability of the magnetotail. In section 5 we test our idea by examining a quasi-steady magnetotail modeled by the RCM-Dungey code, a modified Rice Convection Model with a force balancing scheme. We further discuss in section 6 implications for the mapping of auroral arcs. Section 7 is a summary.

2. Entropy Parameter and Field-Aligned Currents

In this study we assume that the magnetic configuration is symmetric with respect to the equatorial plane, and we are concerned only with the bounce-averaged motion of particles. The ions have finite kinetic energies and undergo magnetic/curvature drift as well as electric drift. We also assume that the ion pressure remains isotropic as they drift. In contrast, the electrons are cold, and accordingly, their motion across the magnetic field is only the electric drift. They are assumed to be the exclusive carriers of FACs. The assumption of cold electrons is not essential for the present study, but it helps to simplify the discussion. We also assume that the plasma convection is much slower than the sound velocity and its change is gradual in both space and time, and therefore, we disregard the inertia current. Accordingly we consider only the pressure gradient current for the closure of FACs in the magnetosphere.

The bounce-averaged drift velocity of ions with kinetic energy w is

$$\boldsymbol{v}(w) = \frac{\boldsymbol{E}\times\boldsymbol{b}}{B_{eq}} - \frac{2w}{3eB_{eq}}\,\boldsymbol{b}\times\nabla \ln V \tag{1}$$

[e.g., *Harel et al*., 1981; *Wolf*, 1983]. Here $\boldsymbol{E}$ is the equatorial electric field, $\boldsymbol{b}$ is the unit vector along the magnetic field $\boldsymbol{b}=\boldsymbol{B}/B$ at the equator, V is the unit flux volume ($=\int \frac{1}{B} ds$; s is a field-aligned coordinate), B_{eq} is the total magnetic field at the equator, w is the ion energy, and e is the unit electric charge. The nabla ∇ operates in the equatorial plane. In the right-hand side of (1), the first term represents the electric drift, and the second term represents the magnetic gradient and curvature drift. For the rest of this section and the Appendix A we assume $\gamma = 5/3$. Using the adiabatic invariant $\lambda = wV^{2/3}$ (1) can be rewritten as

$$\boldsymbol{v}(\lambda) = \frac{\boldsymbol{E}\times\boldsymbol{b}}{B_{eq}} + \frac{\lambda}{eB_{eq}}\,\boldsymbol{b}\times\nabla V^{-2/3} \tag{2}$$

We assume that the distribution function at location $\boldsymbol{x}$ at time t, $F=F(\lambda, \boldsymbol{x}, t)$, is constant along the drift path, and it is expressed as

$$\left(\frac{\partial}{\partial t} + \boldsymbol{v}\cdot\nabla\right) F(\lambda,\ \boldsymbol{x}, t) = 0 \tag{3}$$

where the gradient is taken at constant λ and, following *Liu* [2006], the distribution function is normalized using the ion density $n=n(\boldsymbol{x}, t)$ so that

$$n = \int_0^\infty F w^{1/2} dw = V^{-1}\int_0^\infty F(\lambda)\lambda^{1/2} d\lambda \tag{4}$$

The flux tube entropy parameter $pV^{5/3}$ is written as

$$pV^{5/3} = \frac{2}{3}\int_0^\infty F(\lambda)\lambda^{3/2} d\lambda \tag{5}$$

where p is the plasma pressure. We show in the Appendix A that multiplying (3) by $\lambda^{3/2}$ and integrating over λ gives

$$\left(\frac{\partial}{\partial t} + \frac{\boldsymbol{E}\times\boldsymbol{b}}{B_{eq}}\cdot\nabla\right) pV^{5/3} = \frac{4}{9}\frac{\boldsymbol{b}\times\nabla V}{eB_{eq}V^{5/3}}\cdot\nabla\left(V^{7/3}S + \langle\lambda\rangle^2 nV\right) \tag{6}$$

where we introduced the heat flux parameter S [*Liu*, 2006], which is defined as

$$S = \int F(w)(w - \langle w \rangle)^2 w^{1/2} dw = V^{-7/3} \int F(\lambda)\left(\lambda^{5/2} - \langle \lambda \rangle^2 \lambda^{1/2}\right) d\lambda \tag{7}$$

where $\langle \lambda \rangle$ is the $\lambda^{1/2}$-weighted average of λ:

$$\langle \lambda \rangle = \frac{\int_0^\infty \lambda^{3/2} F d\lambda}{\int_0^\infty \lambda^{1/2} F d\lambda} \tag{8}$$

Equation (6) indicates that $pV^{5/3}$ is not constant along the electric drift, but it changes because of the magnetic drift of particles. In general the right-hand side of (6) depends not only on the spatial distribution of macroscopic quantities such as p and B_{eq} but also on the distribution function of particles (see (7)). In the Appendix A we show that if $F(\lambda)$ is a κ function (6) becomes

$$\left(\frac{\partial}{\partial t} + \frac{\boldsymbol{E} \times \boldsymbol{b}}{B_{eq}} \cdot \nabla\right) pV^{5/3} = \frac{5}{3} \frac{\left(\kappa - \frac{3}{2}\right)}{\left(\kappa - \frac{5}{2}\right)} \frac{T}{eB_{eq}} [\boldsymbol{b} \cdot \nabla \ln(V) \times \nabla \ln(pT)] pV^{5/3} \tag{9}$$

where $T = p/n$. The convergence of the λ integrals requires that κ always be greater than 5/2, which is apparently supported by the observation [e.g., *Christon et al.*, 1989]. Now we consider the vector product $\nabla \ln(V) \times \nabla \ln(pT) = \nabla \ln(V) \times \nabla \ln(p) + \nabla \ln(V) \times \nabla \ln(T)$ from the geometrical point of view. In general both n and T increase earthward, and therefore, $\nabla \ln(p)$ is typically larger than $\nabla \ln(T)$ in magnitude. We also note that if the transport is adiabatic, the energies of particles mirroring at the equator and close to Earth depend on B_{eq} (betatron acceleration) and $1/\int ds$ (Fermi acceleration), respectively. It is therefore expected that the local value of T is better correlated with V ($= \int \frac{1}{B} ds$) than n is, and accordingly, $\nabla \ln(T)$ is more aligned with $\nabla \ln(V)$ than $\nabla \ln(n)$ is. Here based on a simple consideration of the geometry of the three vectors, $\nabla \ln(V)$, $\nabla \ln(T)$, and $\nabla \ln(p) = \nabla \ln(T) + \nabla \ln(n)$, we note that even if $\nabla \ln(V) \times \nabla \ln(p)$ and $\nabla \ln(V) \times \nabla \ln(T)$ have opposite signs, the former is larger than the latter in magnitude more often than it is not. We therefore assume that $\nabla \ln(V) \times \nabla \ln(p)$ determines the sign of the right-hand side of (9).

The *Vasyliunas* [1970] equation

$$\frac{J_{||,i}}{B_i} = \frac{1}{2B_{eq}} (\nabla V \times \nabla p) \cdot \boldsymbol{b} = \frac{pV}{2B_{eq}} \boldsymbol{b} \cdot \nabla \ln(V) \times \nabla \ln(p) \tag{10}$$

relates $\nabla \ln(V) \times \nabla \ln(p)$ to the FAC density at the magnetic footprint at the ionosphere $J_{||,i}$, which is positive and negative if FACs flow into and out of the ionosphere, respectively. B_i is the total magnetic field at the ionospheric footprint, and we assume that the FAC distribution is symmetric between the two hemispheres. Now (9) can be expressed as

$$\frac{\partial}{\partial t}\left(pV^{5/3}\right) + \frac{\boldsymbol{E} \times \boldsymbol{b}}{B_{eq}} \cdot \nabla\left(pV^{5/3}\right) = A(\boldsymbol{x}, t) J_{||,i} \tag{11}$$

Under the aforementioned assumption regarding the right-hand side of (9), $A(\boldsymbol{x}, t)$ is positive for any $(\boldsymbol{x}, t)$. That is, the sign of the right-hand side of (11) is determined by $J_{||,i}$. This is equivalent to assuming that the divergence of the heat flux due to the magnetic gradient has the same sign as the divergence of the number flux and therefore the divergence of the pressure gradient current (as the magnetization current is divergence free).

Finally, let us evaluate the effect of the magnetic drift on the change of $pV^{5/3}$. If we simply replace $\nabla \ln(V) \times \nabla \ln(pT)$ with $\nabla \ln(V) \times \nabla \ln(p)$, (9) can be rewritten with (10) as

$$\frac{\partial}{\partial t}\left(pV^{5/3}\right) + \frac{\boldsymbol{E} \times \boldsymbol{b}}{B_{eq}} \cdot \nabla\left(pV^{5/3}\right) = \frac{5}{3} \frac{\left(\kappa - \frac{3}{2}\right)}{\left(\kappa - \frac{5}{2}\right)} \frac{J_{||,i}}{eB_i} \frac{2}{nV} \left(pV^{5/3}\right) \tag{12}$$

If the (partial) time derivative of $pV^{5/3}$ on the left-hand side of (12) balances with the right-hand side, the characteristic timescale τ is expressed as

$$\tau = \frac{3}{5} \frac{\left(\kappa - \frac{5}{2}\right)}{\left(\kappa - \frac{3}{2}\right)} \frac{\frac{nV}{2}}{\frac{J_{||,i}}{eB_i}} \tag{13}$$

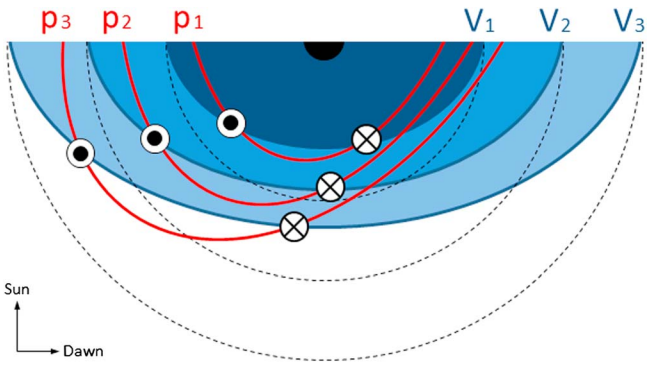

Figure 1. The divergence of the pressure gradient current in the equatorial plane. Three levels of V, $V_1 < V_2 < V_3$, are shown by three areas shaded by in different bluish colors, whereas three equi-contours of p, $p_1 > p_2 > p_3$, are shown by red lines. The pressure gradient current closes with FACs flowing toward and out of the ionosphere at the duskward and dawnward intersects of V_i and p_i (i: 1, 2, 3). The duskward skewing of the equi-p contours make the area of the upward FAC extends from the premidnight plasma sheet to the postmidnight near-Earth region.

Here $\frac{nV}{2}$ represents the total number of ions in the unit flux tube in one hemisphere, whereas $\frac{J_{\|,i}}{eB_i}$ represents the rate at which electrons enter or leave the flux tube at the ionosphere, which equals the rate at which ions enter or leave the flux tube in the magnetosphere. The coefficient $\frac{3}{5}\frac{\left(\kappa-\frac{5}{2}\right)}{\left(\kappa-\frac{3}{2}\right)}$ is 0.4–0.5 for $\kappa = 5$–7 [*Christon et al.*, 1989]. For $n = 0.2\,\mathrm{cm}^{-3}$, $V = 1\,R_E/\mathrm{nT}$ [*Wang et al.*, 2009], $J_{\|}$, i = 1 μA/m^2 [e.g., *Iijima and Potemra*, 1976], and $B_i = 50{,}000$ nT, τ is estimated at 40 min. If the right-hand side of (12) balances with the advective change of $pV^{5/3}$, the second term on the left-hand side, the corresponding spatial scale $L\left(=\left|\frac{\boldsymbol{E}\times\boldsymbol{b}}{B_{eq}}\tau\right|\right)$ is estimated at $6\,R_E$ for an equatorial electric field of 0.1 mV/m (30 kV over $50\,R_E$) and a total magnetic field of 5 nT; more precisely, this is the spatial scale of $\nabla(pV^{5/3})$ projected to the direction of the convection. These estimates are comparable to the temporal and spatial scales of the convection in the plasma sheet. That is, the flux-volume entropy $pV^{5/3}$ can change significantly due to the divergence of the magnetic drift (as described as the FAC closure) on the timescale and spatial scale of convection.

3. Pressure Distribution (Equi-*p* Contours)

The polarities of FACs are determined by the relative directions of ∇p and ∇V (equation (10)). The terrestrial dipole field is axisymmetric, and the reduction of the equatorial magnetic field by the tail current enhances the unit flux volume in the near-Earth magnetotail. Therefore, in the near-Earth region (where the terrestrial dipole contributes to the local magnetic field), the equi-V contours extend less outward at midnight than at the flanks. In contrast, the equatorial distribution of p is determined by the force balance with the magnetic stress, and as the magnetic field is stretched antisunward in the plasma sheet, the equi-p contours extend more outward at midnight than at the flanks. Therefore, the equi-p contours should extend farther out of the equi-V contours in the plasma sheet. If the contours of p and V are symmetric with respect to midnight ($Y = 0$), the FAC flows to and out of the ionosphere in the premidnight and postmidnight sectors, respectively (see (10)). The polarity is the same as that of the R2 system.

In reality, however, the polar distribution of FACs is not symmetric with respect to the midnight meridian, but the premidnight upward R1 current and postmidnight R2 current are spatially continuous [*Iijima and Potemra*, 1976]. This FAC distribution can be explained by assuming that the pressure distribution is skewed duskward in the magnetosphere, which is schematically explained in Figure 1. In this figure three levels of V, $V_1 < V_2 < V_3$, are shown by three areas shaded by different bluish colors, whereas three equicontours of p, $p_1 > p_2 > p_3$, are shown by red curves. The contours V_i and p_i ($i = 1, 2, 3$) intersect at two locations. The pressure gradient current converges at the duskside intersect, and it closes with a FAC flowing into the ionosphere there. At the dawnside intersect, it diverges and closes with a FAC flowing out of the ionosphere. Therefore, the polarity of each FAC pair is the same as that of the R2 system. However, as the equi-p contour skews duskward with increasing radial distance, the region of upward FACs extends from postmidnight to premidnight. The premidnight and postmidnight parts of this upward FAC may be considered as the premidnight R1 and postmidnight R2 currents, respectively. The duskward pressure gradient is observed persistently at 10–12 R_E in the quiet time nightside magnetosphere, suggesting that the local closure of the tail current with an upward FAC [*Xing et al.*, 2009]. This observational result strongly supports the skewing of the equi-p contours, which we consider essential for the closure of the nightside FACs in the near-Earth region.

4. Convection and Interchange Stability

In this section we seek to reconstruct the (quasi-)steady convection in the plasma sheet based on the interchange stability. We consider the ordinary two-cell pattern of magnetospheric convection, which consists of duskside and dawnside convection cells, and we focus on the return flow parts of those convection cells in the midnight sector of the plasma sheet. We assume that the magnetosphere is in a steady state. Accordingly, we disregard the first term on the left-hand side of (11), and we have

$$\frac{\boldsymbol{E}\times\boldsymbol{b}}{B_{eq}}\cdot\nabla(pV^{\gamma}) = A(\boldsymbol{x},t)J_{||,i} \tag{14}$$

From now on we use γ as heat capacity ratio again for notational simplicity. The electric field is described by the statistic electric potential Φ ($\boldsymbol{E}=-\nabla\Phi$), and the local convection flow (electric drift) is parallel to the equi-Φ contour.

For the plasma sheet to be interchange stable, the angle between $\nabla(pV^{\gamma})$ and ∇V has to be less than 90° [*Xing and Wolf*, 2007], that is,

$$\nabla(pV^{\gamma})\cdot\nabla V > 0 \tag{15}$$

From a purely mathematical point of view, (14) and (15) indicate that depending on the sign of $J_{||,i}$, $\frac{\boldsymbol{E}\times\boldsymbol{b}}{B}$ and ∇V have to be in the same hemisphere (for a positive inner product) or in the opposite hemispheres (for a negative inner product) with respect to the direction of $\nabla(pV^{\gamma})$. This may not appear to be a serious constraint.

In reality, however, (14) and (15) impose a serious constraint on the direction of convection. In the first approximation, the flux volume V decreases primarily sunward in the plasma sheet, and off the noon-midnight meridian, the direction of the V reduction changes gradually to radially earthward in the near-Earth region. This is also the case for pV^{γ} because its spatial distribution largely reflects that of V, although p may vary in the Y or azimuthal direction more significantly than V does. In addition, the X component of the return convection flow, $\frac{\boldsymbol{E}\times\boldsymbol{b}}{B}$, has to be positive (sunward) outside of the shielding region, that is, in the equatorial region corresponding to the R1 system, although in the region corresponding to the R2 system $\frac{\boldsymbol{E}\times\boldsymbol{b}}{B}$ may be directed azimuthally to go around Earth. Therefore, $-\nabla V$, $-\nabla(pV^{\gamma})$, and $\frac{\boldsymbol{E}\times\boldsymbol{b}}{B}$ are directed in similar directions overall in the plasma sheet.

If $J_{||,i}$ is negative, that is, the FAC polarity is upward (out of the ionosphere), (14) tells us that pV^{γ} decreases in the direction of convection, and therefore, the stability condition (15) does not impose a serious constraint on the direction of convection, and it leaves us flexibility in constructing an interchange stable convection pattern. It is therefore reasonable to assume that the convection in the upward FAC region is established so that the sunward return of the global convection (i.e., the convection toward the dayside magnetopause) becomes most efficient. The situation is rather different for the region of downward FACs, where pV^{γ} increases in the direction of convection. If the convection is primarily sunward (or earthward) as we usually expect for the return convection flow, pV^{γ} increases as V decreases (i.e., $\nabla(pV^{\gamma})\cdot\nabla V<0$), which results in the interchange instability. In other words, if the plasma sheet is interchange stable, the convection flow must deflect significantly from the direction of $\nabla pV^{5/3}$.

Now we seek to reconstruct the convection in the plasma sheet. We start with the dusk cell. In the near-Earth region ∇V is directed radially outward, and the FAC, that is, the R2 current, flows into the ionosphere (blue-shaded area in the premidnight sector in Figure 2). For this FAC polarity, $\frac{\boldsymbol{E}\times\boldsymbol{b}}{B}\cdot\nabla(pV^{\gamma})>0$ (see (14)). If the convection has an earthward component, pV^{γ} increases earthward as V decreases, resulting in $\nabla(pV^{\gamma})\cdot\nabla V<0$, that is, the interchange instability. On the other hand, it is unlikely that the return convection has a large outward component. Therefore, the convection has to be mostly azimuthal and be directed duskward. The associated duskward increase in pV^{γ} along the convection flow is consistent with the duskward skewing of the equi-p contours (section 3).

Farther down the tail, the duskside convection cell is collocated with the upward R1 current; see the red-shaded area in the premidnight sector in Figure 2, which extends to the postmidnight near-Earth region (section 3). For this FAC polarity the stability condition alone does not impose a serious constraint on the direction of convection. However, as we will discuss soon, the interchange stability requires the dawn-cell convection to deflect dawnward in the corresponding R1 current area. It is therefore reasonable to consider that the

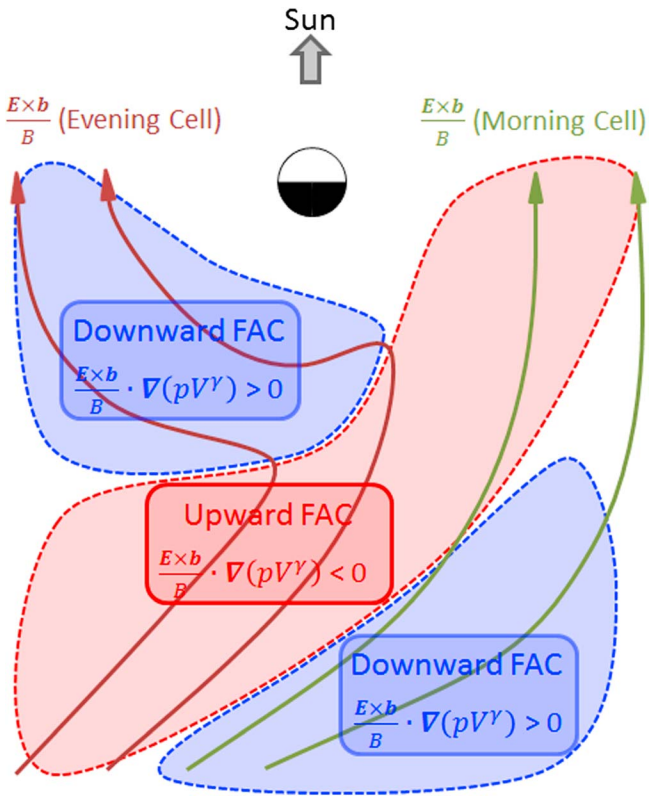

Figure 2. The schematic explanation of the correspondence between the FAC polarities and convection flows expected for the quasi-steady interchange stable plasma sheet. The equatorial distributions of upward (red) and downward (blue) FACs are shown along with representative convection flow lines of the evening (reddish brown) and morning (yellow-green) cells.

dusk-cell convection also deflects dawnward. Otherwise, the convection would be weaker around the demarcation between the dawn and dusk convection cells, for which we cannot think of any physical reason or observational evidence. Thus, the equi-Φ contours of the dusk convection cell deflect dawnward in the upward R1 region, make duskward turns around the R1-R2 transition, and then extend azimuthally in the downward R2 region. Since the R1 and R2 currents are adjacent to each other (as shown by the low-altitude observation [e.g., *Iijima and Potemra*, 1976]), this duskward turn of the convection flow is expected to take place abruptly in space (relative to the scale of the R1 and R2 currents), which is presumably the magnetospheric counterpart of the Harang reversal.

Now we discuss the dawn cell, for which the R1 and R2 currents flow to and out of the ionosphere, respectively. For the plasma sheet area corresponding to the downward R1 current, pV^γ increases in the direction of convection, whereas V decreases roughly sunward. Therefore, the interchange stability (15) requires that the convection deflect significantly from sunward. This deflection has to be dawnward. If it is duskward, instead, the convection has to be pulled back dawnward in the near-Earth region. It is not conceivable that such dawnward convection coexists with the duskward convection of the dusk cell in the same region, which we discussed above. Closer to Earth, where the R2 current flows out of the ionosphere, the direction of convection is not constrained by the interchange stability. We therefore suggest that the convection is directed sunward (as expected for the return flow) in the R2 part of the dawn cell following the dawnward-deflecting convection in its R1 part.

We emphasize that the above discussion does not mean in any sense that the ionosphere does not play any essential role, and the plasma sheet convection is determined solely by the interchange stability of the plasma sheet. The magnetosphere reaches a steady state through its interaction with the ionosphere, and the spatial distributions of magnetospheric and ionospheric quantities (e.g., electrostatic potential, plasma pressure, magnetic field, FACs, and ionospheric conductances) have to be consistent with each other [e.g., *Vasyliunas*, 1970]. Therefore, by assuming the distribution of upward and downward FACs, our model reflects the effects of the ionosphere such as the distribution of ionospheric conductance. Here we should make two points regarding the convection pattern that we deduced (Figure 2).

First we note that the deduced convection pattern, if mapped to the ionosphere, is consistent with the assumed FAC distribution. In the ionosphere the convection electric field is directed equatorward and poleward on the poleward and equatorward sides of the convection reversal. This convergence of the electric field is generally accompanied by the convergence of Pedersen currents, which close with an upward FAC; though, the conductance gradient is also important as we will discuss below. The eastward convection on the poleward side and the westward convection on the equatorward side are confined in latitude, and accordingly, they are both bounded by downward FACs. Thus the three sheet structure of FACs is expected in the longitudinal sector of the Harang reversal. On the dawn side, in contrast, the convection is directed

eastward throughout the auroral oval, and the associated equatorward electric field drives a Pedersen current, which closes with downward and upward FACs on the poleward and equatorward sides. Thus, the overall FAC distribution expected from the deduced convection is consistent with the FAC distribution we initially assumed.

Second, the location of the Harang reversal relative to the R1 and R2 currents is consistent with the low-altitude observation. Our model predicts that the Harang reversal is located inside the upward R1 FAC but close to its equatorward boundary, which is very consistent with the satellite observation made above the ionosphere [*Zou et al*., 2009a, 2009b]. This can be explained in terms of the latitudinal gradient of ionospheric conductance induced by electron precipitation. In the premidnight sector the average energy flux of electron precipitation in the upward R1 current is larger than that in the downward R2 current by almost an order of magnitude because of auroral acceleration, and the change often takes place steplike around the demarcation between the two current systems [*Ohtani et al*., 2009; *Zou et al*., 2009a, Figure 4]. Therefore, the ionospheric conductance changes sharply with latitude around the Harang reversal, and on the equatorward side of the reversal the intensity of the poleward Pedersen current decreases with decreasing latitude. Accordingly the Pedersen current diverges, and it closes with a downward FAC. Thus, the downward FAC starts equatorward of, but close to, the Harang reversal primarily because of the conductance gradient. Interestingly, the previous modeling studies with a potential solver also showed that a convection structure resembling the Harang reversal appears at the conductance gradient in the premidnight sector [e.g., *Kamide and Matsushita*, 1979]. Thus, the results of all different approaches (i.e., our physics-based model, satellite observations, and potential solver) converge regarding the interrelationship among the distributions of convection, FAC, and ionospheric conductance around the Harang reversal, which we will further confirm with a numerical model in the next section.

We also note that if the Harang reversal is located close to the equatorward edge of the upward FAC, the eastward ionospheric convection can extend through the predominant part of the upward FAC sheet, and therefore, the sunward return convection in the plasma sheet (Figure 2) is realized most efficiently, which may reflect the minimum energy state of the magnetosphere for a given external condition. The idea is consistent with the fact that the Harang reversal very often takes place as a structure of the steady convection (section 1).

5. Comparision With a Modeled Plasma Sheet

In this section, using a modeled plasma sheet, we test our analytical deductions about the interrelationship among the convection flow, FAC polarities, and pV^{γ}. More specifically, we examine the simulation results of the Rice Convection Model (RCM) [*Toffoletto et al*., 2003] combined with a modified Dungey force-balanced magnetic field solver [*Schulz and Chen*, 2008; *Gkioulidou et al*., 2011]. The coupled RCM-Dungey model calculates the bounce-averaged electric and magnetic drifts of ions and electrons within self-consistently computed electric and magnetic fields assuming, as we did in our analysis, that the pitch-angle distributions are always isotropic and the plasma flow across the magnetic field is slow.

The self-consistent electric field is obtained from the current continuity equation both in the magnetosphere and ionosphere [*Vasyliunas*, 1970]:

$$\nabla \cdot [\Sigma \cdot \nabla \Phi] = -J_{||,i} \sin(I) = \frac{B_i}{2B_{eq}} \boldsymbol{b} \cdot (\nabla p \times \nabla V) \sin(I) \tag{16}$$

where Σ is the field-line integrated ionospheric conductance tensor including both the Hall and Pedersen conductances and I is the dip angle of the magnetic field at the ionosphere. The conductance consists of two contributions: (i) Solar-EUV-generated conductance that is estimated from the IRI-90 empirical ionosphere driven by $F_{10.7}$ and the *Ap* index and (ii) auroral conductance, which depends on electron precipitation estimated from the *Chen and Schulz* [2001] MLT-dependent scattering rate model (for more details on the calculation of auroral conductances see *Gkioulidou et al*. [2012]). We adopted a Dirichlet boundary condition for the potential at the high-latitude boundary; the overall strength of convection is determined by the cross-polar cap potential $\Delta\Phi_{PC}$.

The location of the outer boundary is specified at a 15 R_E circle centered at $X = -5\,R_E$ and $Y = 0$ in the equatorial plane, which therefore reaches $X = -20\,R_E$ at midnight and $|Y| = 15\,\mathrm{R_E}$ on the dawn and dusk sides. The latitudes in the ionosphere that map to the outer boundary vary as the magnetic configuration

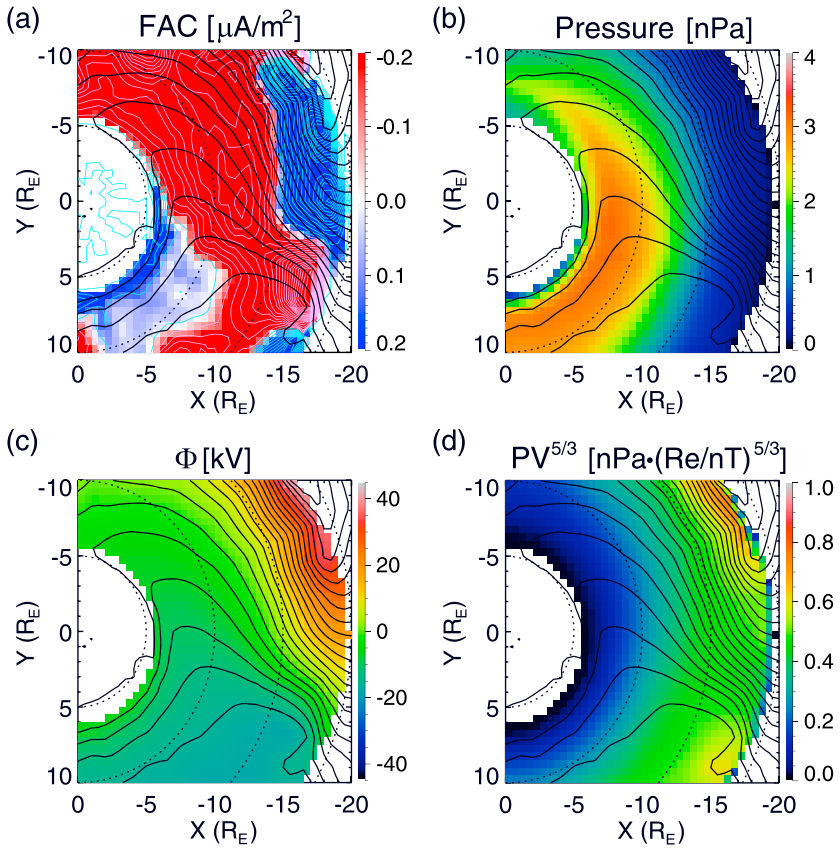

Figure 3. The equatorial ($0 \geq X \geq -20\,R_E$ and $|Y| \leq 10\,R_E$) distributions of (a) the ionospheric FAC density mapped to the equatorial plane with its contours (the maximum FAC densities are 2.5 and 4.9 $\mu A/m^2$ for the upward (negative, red) and downward (positive, blue) FACs, respectively, and the contours are separated by 0.12 $\mu A/m^2$), (b) plasma pressure, p, (c) electrostatic potential, Φ, and (d) $pV^{\hat{\gamma}}$ in units of nPa $\cdot$ $(R_E/\mathrm{nT})^{5/3}$ in color along with the equi-Φ contours (for each panel) of the quasi-steady plasma sheet reproduced by the RCM-Dungey model (see text for details).

changes. The inner boundary is at $r = 2\,R_E$. Along the outer boundary the proton and electron distributions at different MLTs are specified by fitting two-component kappa distributions to Geotail measurements (unpublished result); in this particular simulation we used plasma boundary conditions for moderately high solar wind driving.

We ran the RCM-Dungey model with $\Delta\Phi_{PC}$ of 30 kV for five simulation hours. Then we increased $\Delta\Phi_{PC}$ to 90 kV and kept it constant for the next 3.5 h. The magnetic field was updated every 10 min to maintain force balance with the plasma pressure. By the end of this 8.5 h period the simulation reaches a quasi steady state, in which no further changes are evident in the evolution of the system properties (e.g., the distributions of FAC, pressure flux tube volume, and electric field). In the following we will examine thus achieved steady state plasma sheet focusing on the area at $-20 \leq X \leq 0\,R_E$ and $|Y| \leq 10\,R_E$.

Figure 3a shows in color the equatorial distribution of the ionospheric FAC density mapped to the equatorial plane with reddish and bluish tones for upward (out of the ionosphere) and downward (to the ionosphere) FACs, respectively. In the near-Earth region the FAC flows out of and into the ionosphere in the postmidnight and premidnight sectors, respectively, and the polarities are just the opposite farther down the tail. The area of upward FACs extends continuously from near the outer boundary at premidnight to closer to Earth at postmidnight. The polarities of FACs and their spatial distribution are consistent with those of the R1 and R2 currents observed above the ionosphere [*Iijima and Potemra*, 1976]. The plasma pressure p, the sum of the ion and electron thermal pressures, is shown in color in Figure 3b, which shows that the p distribution is significantly skewed duskward in the near-Earth region. This p distribution is consistent with the FAC distribution as we discussed in section 3.

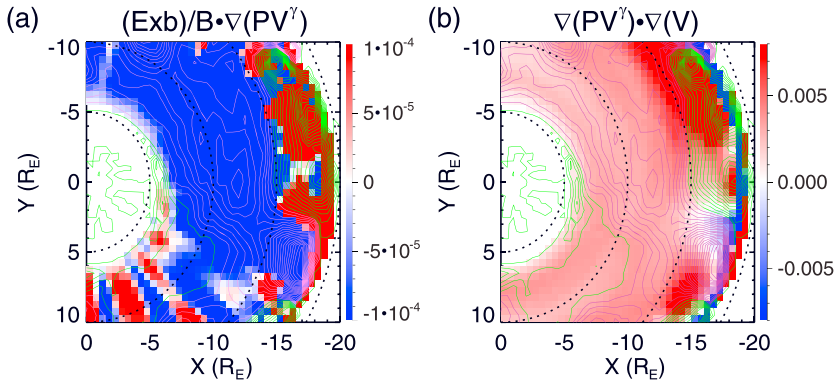

Figure 4. The equatorial ($0 \geq X \geq -20\,R_E$ and $|Y| \leq 10\,R_E$) distributions of (a) $\frac{\boldsymbol{E}\times\boldsymbol{b}}{B}\cdot\nabla(pV^{\gamma})$ and (b) $\nabla(pV^{\gamma})\cdot\nabla V$ in color along with the contours of downward (magenta) and upward (green) FAC densities of the quasi-steady plasma sheet reproduced by the RCM-Dungey model (see text for details). Those inner products are calculated with $\frac{\boldsymbol{E}\times\boldsymbol{b}}{B}$, V, and p in units of km/s, R_E/nT, and nPa, respectively, and with $\gamma = 5/3$.

Figure 3c shows in color the electrostatic potential Φ along with its contours. The distribution is significantly asymmetric with respect to midnight. The Φ contours first head dawnward from the outer boundary. Those originating from the midnight-postmidnight sector then go around Earth through the morning side, which correspond to the return flow of the dawn convection cell. The equi-Φ contours originating from the premidnight sector, however, make abrupt duskward turns in the near-Earth region after the initial dawnward excursion, and then they roughly proceed azimuthally at constant radial distances.

Those equi-Φ contours are superposed on the top of the FAC density in Figure 3a. In the near-Earth region the azimuthally duskward convection of the dusk convection cell is collocated with the downward R2 current, and the preceding abrupt duskward turnings take place in the vicinity, but slightly on the upstream side, of the demarcation between the upward and downward FACs. In the region of the dawnside downward R1 current farther down the tail, the convection is directed azimuthally dawnward. Note that the convection flow is deflected dawnward immediately inside the outer boundary, which can be attributed to the imposed boundary condition of Φ; equi-Φ contours have to cross the boundary accordingly to the distribution of Φ along the boundary, which constrains the orientation of equi-Φ contours. Otherwise, the convection flow has a significant sunward component only in the region of the upward FACs, which is consistent with the inference that we made in section 4.

The distribution of pV^{γ} is shown in the same way in Figure 3d. As expected, pV^{γ} increases outward reflecting the outward increase in V. We further expect that pV^{γ} increases and decreases in the direction of convection where the FAC flows to and out of the ionosphere, respectively. Figure 4a shows the equatorial distribution of $\frac{\boldsymbol{E}\times\boldsymbol{b}}{B}\cdot\nabla(pV^{\gamma})$ in color. Superposed on the top of this inner product are the equicontours of the FAC density. The contours are green for downward FACs and magenta for upward FACs. In general $\frac{\boldsymbol{E}\times\boldsymbol{b}}{B}\cdot\nabla(pV^{\gamma})$ is positive and negative for downward and upward FACs, respectively, although the correspondence is not perfect especially in the dusk sector, where this inner product change periodically in longitude for an unknown reason. We made two assumptions to obtain (14) from (11); one is that the magnetotail is in a steady state and the other is that the divergence of the ion energy flux has the same sign as $J_{||,i}$. Figure 4a indicates that these two assumptions hold rather well for this modeled plasma sheet.

Figure 4b shows $\nabla(pV^{\gamma})\cdot\nabla V$ in the same way. Except for a very limited area along the outer boundary, $\nabla(pV^{\gamma})\cdot\nabla V$ is positive (shown by reddish colors) throughout the system indicating that the modeled plasma sheet is interchange stable. The areas of negative $\nabla(pV^{\gamma})\cdot\nabla V$ (shown by bluish colors) near the outer boundary are collocated exclusively with downward FACs, for which the interchange stability imposes a far more significant constraint on the directions of convection flow, $\nabla(pV^{\gamma})$, and ∇V than for upward FACs. This negative $\nabla(pV^{\gamma})\cdot\nabla V$ is presumably a boundary effect. Whereas we specify Φ and p separately along the outer boundary, those two quantities are not completely independent. The profile of Φ not only determines the electric field (more precisely, its component parallel to the outer boundary) but also places a constraint on the FAC distribution through the current closure at the ionosphere and therefore on the pressure gradient in the plasma sheet as the FACs close with the pressure gradient current in the magnetosphere. It is likely that

for the given profiles of p and Φ along the outer boundary, the M-I system is not able to adjust itself for the interchange stability immediately inside the outer boundary.

The associations we found among FACs, convection, and $pV^{\prime}$ are consistent with the requirements for the interchange stability of the plasma sheet in the presence of the R1 and R2 currents (section 4). A similar simulation but with the Rice Convection Model-Equilibrium (RCM-E) for a steady magnetospheric convection event was reported by *Yang et al*. [2014]. Their simulated convection pattern also reveals the Harang reversal, and its location relative to the FAC distribution is consistent with our expectation (see Figure 5 of their paper). Although some specifics of their result as well as ours probably depend on the setting of the simulation, the R1 and R2 systems are most fundamental features of the magnetosphere. We therefore conclude that the Harang reversal is a general solution for the interchange stability of the (quasi-)steady magnetotail.

6. Implications for the Mapping of Auroral Arcs

The present study also provides an important insight into the mapping of auroral arcs to the equatorial plane. Auroral arcs are very often aligned in the east-west direction especially before substorm onsets [e.g., *Akasofu*, 1964] and so are the equi-Φ contours in the auroral oval. Therefore, the angles between auroral arcs and equi-Φ contours should be generally small, and the equi-Φ contours in the equatorial plane serve as a reference for mapping auroral arcs to the plasma sheet as far as the field-aligned potential difference is small.

We are most interested in the premidnight sector, where the auroral oval is characterized by monoenergetic rather than diffuse, electron precipitation and the convection pattern is characterized by the Harang reversal. In this MLT sector most discrete auroral arcs are embedded in the upward R1 current [*Ohtani et al*., 2010]. Based on the consideration of the equi-Φ contours in section 4, we suggest that those arcs magnetically mapped to the plasma sheet are oriented in the Sun-Earth direction rather than in the azimuthal direction. It is possible that they are preferably oriented in the [$+x$, $-y$]-to-[$-x$, $+y$] direction following the expected dawnward deflection of the equi-Φ contours in the R1 part of the plasma sheet.

Special attention has been paid to the mapping of the onset arc, the arc that breaks up at a substorm onset, as it is critical for understanding the substorm initiation. Auroral substorms often start at the most equatorward arc in the premidnight sector [*Akasofu*, 1964]. It has also been known for many years that the onset arc is located around the Harang reversal [e.g., *Nielsen and Greenwald*, 1979] (see also section 1). In the dusk-midnight sector the most equatorward arc is located very often inside the upward R1 current but close to its boundary with the downward R2 current [*Ohtani et al*., 2010], which is also confirmed specifically for the substorm growth phase [*Jiang et al*., 2015]. Therefore, during the growth phase, the onset arc mapped to the equatorial plane is likely more inclined from the Sun-Earth direction than auroral arcs farther poleward.

Furthermore, in some events the onset arc was reportedly embedded in the R2 current just prior to the auroral breakup [*Nishimura et al*., 2012; *Motoba et al*., 2015]. If this is the case, its equatorial projection is expected to extend in the azimuthal direction. It is well known that periodic structures often emerge along the onset arc just prior to the auroral breakup, which are referred to as auroral beads [e.g., *Motoba et al*., 2012]. If the arc mapped to the equatorial plane is oriented in the azimuthal direction, such periodic auroral structures presumably correspond to large m number waves propagating azimuthally in the magnetosphere.

7. Summary

In the present study we sought to reconstruct the fundamental features of the plasma sheet convection based on the interrelationship among the plasma convection, FACs, plasma pressure, and magnetic configuration along with the condition for the interchange stability. If the transport of the ions in the plasma sheet is adiabatic and the magnetotail is in a steady state, the advective change of $PV^{\prime}$ by the convection has to balance with the divergence of the energy flux carried by the magnetic drifts of the ions. If this latter effect has the same sign as the divergence of the ion number flux, therefore as the divergence of the tail current, $PV^{\prime}$ has to increase and decrease along the convection path where the FAC flows to and out of the ionosphere, respectively. This requirement, along with the condition of the interchange stability $\nabla(pV^{\prime}) \cdot \nabla V > 0$, imposes an important constraint on the direction of convection, especially for downward FACs, for which the convection flow has to significantly deflect from the direction of ∇V. As a result, for the dawn cell the convection deflects dawnward in the R1 system, and then it proceeds sunward in the R2 system. For the dusk cell, the

convection in the R1 system is directed sunward likely deflecting dawnward, and then it makes a duskward turn followed by the azimuthal convection in the R2 system. This duskward turn takes place in the vicinity of the R1-R2 demarcation, and it presumably corresponds to the Harang reversal. We therefore concluded that the Harang reversal is a general solution for the interchange stability of the steady magnetotail. We verified these outcomes of our theoretical exercise by examining a steady state plasma sheet reproduced by the RCM-Dungey model. Using the equi-Φ contours as a reference we also suggested that in the premidnight sector auroral arcs magnetically mapped to the equator are oriented azimuthally if they are located in the R2 current and in the Sun-Earth direction if located in the R1 current. Since the auroral breakup very often takes place around the Harang reversal, we suggest that this mapping along with the close link between the Harang reversal and the interchange stability provides an important clue for understanding the substorm initiation process.

Appendix A

The evolution of the distribution function in lossless adiabatic convection of an isotropic plasma is, from (2) and (3), given by

$$\left[\frac{\partial}{\partial t}+\left(\boldsymbol{u}_{\mathrm{E}}+\frac{\lambda \boldsymbol{b}\times\nabla V^{-2/3}}{eB_{eq}}\right)\cdot\nabla\right]F(\lambda,\ \boldsymbol{x},t)=0 \tag{A1}$$

where $\boldsymbol{u}_{\mathrm{E}}=\frac{\boldsymbol{E}\times\boldsymbol{b}}{B_{eq}}$. Equation (A1) means that the distribution function in a particle's vicinity in phase space remains constant as the particle drifts. Note that the gradient in (A1) is taken at constant λ, not at constant energy. Multiplying (A1) by $\lambda^{3/2}$, moving the advection term by the magnetic drift to the right side and integrating over λ, we obtain

$$\left(\frac{\partial}{\partial t}+\boldsymbol{u}_{\mathrm{E}}\cdot\nabla\right)\int_0^\infty\lambda^{3/2}Fd\lambda=-\frac{\boldsymbol{b}\times\nabla V^{-\frac{2}{3}}}{eB_{eq}}\cdot\nabla\int_0^\infty\lambda^{5/2}Fd\lambda \tag{A2}$$

which can be rewritten, with (5), as

$$\left(\frac{\partial}{\partial t}+\boldsymbol{u}_{\mathrm{E}}\cdot\nabla\right)pV^{5/3}=-\frac{2}{3}\frac{\boldsymbol{b}\times\nabla V^{-\frac{2}{3}}}{eB_{eq}}\cdot\nabla\int_0^\infty\lambda^{5/2}Fd\lambda \tag{A3}$$

Using $\langle\lambda\rangle$, the average λ as defined by (8), we can write

$$\begin{aligned}\int_0^\infty\lambda^{5/2}Fd\lambda&=\int_0^\infty\left[(\lambda-\langle\lambda\rangle)^2+2\lambda\langle\lambda\rangle-\langle\lambda\rangle^2\right]\lambda^{1/2}Fd\lambda\\&=\int_0^\infty(\lambda-\langle\lambda\rangle)^2\lambda^{1/2}Fd\lambda+\langle\lambda\rangle^2\int_0^\infty\lambda^{1/2}Fd\lambda\\&=V^{7/3}S+\langle\lambda\rangle^2nV\end{aligned} \tag{A4}$$

where we used the definition of S, (7), along with (4). Substituting (A4) in (A3) gives

$$\left(\frac{\partial}{\partial t}+\boldsymbol{u}_{\mathrm{E}}\cdot\nabla\right)pV^{5/3}=\frac{4}{9}\frac{\boldsymbol{b}\times\nabla V}{eB_{eq}V^{5/3}}\cdot\nabla\left(V^{7/3}S+\langle\lambda\rangle^2nV\right) \tag{A5}$$

which is (6) in section 2.

To evaluate the right side of (A5), we assume F is a κ function with constant κ

$$F(\lambda)=\frac{2nV\Gamma(\kappa+1)}{\sqrt{\pi}(\lambda_0\kappa)^{3/2}\Gamma\left(\kappa-\frac{1}{2}\right)}\frac{1}{\left(1+\frac{\lambda}{\kappa\lambda_0}\right)^{\kappa+1}} \tag{A6}$$

where λ_0 is the λ value corresponding to the most probable energy w_0 (i.e., $\lambda_0 = w_0 V^{2/3}$). We have also used

$$\int_0^\infty \left(1+\frac{\lambda}{\kappa\lambda_0}\right)^{-\kappa-1}\lambda^{1/2}d\lambda = (\kappa\lambda_0)^{3/2}\frac{\sqrt{\pi}\Gamma\left(\kappa-\frac{1}{2}\right)}{2\Gamma(\kappa+1)} \tag{A7}$$

in establishing the normalization. Substituting (A6) in (5) gives

$$pV^{5/3} = n\lambda_0 V\frac{\kappa}{\kappa-\frac{3}{2}} \tag{A8}$$

so that

$$TV^{2/3} = \frac{\lambda_0\kappa}{\kappa-\frac{3}{2}} \tag{A9}$$

and

$$pT = nV^{-4/3}{\lambda_0}^2\left(\frac{\kappa}{\kappa-\frac{3}{2}}\right)^2 \tag{A10}$$

Proceeding to evaluate S, we start by noting that

$$\langle\lambda\rangle = \frac{\int_0^\infty \left(1+\frac{\lambda}{\kappa\lambda_0}\right)^{-\kappa-1}\lambda^{3/2}d\lambda}{\int_0^\infty \left(1+\frac{\lambda}{\kappa\lambda_0}\right)^{-\kappa-1}\lambda^{1/2}d\lambda} = \frac{3\kappa\lambda_0}{2\left(\kappa-\frac{3}{2}\right)} \tag{A11}$$

Using (7), (A6), (A7), (A11), and the fact that

$$\int_0^\infty \left(1+\frac{\lambda}{\kappa\lambda_0}\right)^{-\kappa-1}\lambda^{5/2}d\lambda = \frac{15(\kappa\lambda_0)^{7/2}\sqrt{\pi}\Gamma\left(\kappa-\frac{1}{2}\right)}{8\Gamma(\kappa+1)\left(\kappa-\frac{3}{2}\right)\left(\kappa-\frac{5}{2}\right)} \tag{A12}$$

we find that

$$S = \frac{3nV^{-4/3}{\lambda_0}^2}{2}\frac{\kappa^3}{\left(\kappa-\frac{3}{2}\right)^2\left(\kappa-\frac{5}{2}\right)} \tag{A13}$$

With (A12) and (A13), (A5) becomes

$$\left(\frac{\partial}{\partial t}+\boldsymbol{u}_E\cdot\nabla\right)pV^{5/3} = \frac{4V^{2/3}}{9eB_{eq}}\boldsymbol{b}\times\nabla V\cdot\nabla\left(S+\frac{9}{4}pT\right) \tag{A14}$$

which is slightly different from the result of *Liu* [2006]; see their equation (21). The reason for the difference is not clear to us because *Liu* [2006] includes no derivation of the equation. Further using (A13) along with (A10), (A14) becomes

$$\left(\frac{\partial}{\partial t}+\boldsymbol{u}_E\cdot\nabla\right)pV^{5/3} = \frac{5}{3}\frac{\left(\kappa-\frac{3}{2}\right)}{\left(\kappa-\frac{5}{2}\right)}\frac{T}{eB_{eq}}[\boldsymbol{b}\cdot\nabla\ln(V)\times\nabla\ln(pT)]pV^{5/3} \tag{A15}$$

which is (9) in section 2.

Acknowledgments
Work at JHU/APL was supported by NASA grant NNX12AJ52G and NSF grant ATM-1104338. Work at UCLA was supported by NASA grant NNX11AJ12G and NSF grant ATM-1003595. Work at Rice University was supported by NASA LWS grant NNX14AE04G. Data required for reproducing the included figures of the simulation results are available upon request.

References

Akasofu, S.-I. (1964), The development of the auroral substorm, *Planet. Space Sci.*, *12*, 273.
Angelopoulos, V., C. F. Kennel, F. V. Coroniti, R. Pellat, M. G. Kivelson, R. J. Walker, C. T. Russell, W. Baumjohann, W. C. Feldman, and J. T. Gosling (1994), Statistical characteristics of bursty bulk flow events, *J. Geophys. Res.*, *99*(A11), 21,257–21,280, doi:10.1029/94JA01263.
Bristow, W. A., and P. Jensen (2007), A superposed epoch study of SuperDARN convection observations during substorms, *J. Geophys. Res.*, *112*, A06232, doi:10.1029/2006JA012049.
Chen, M. W., and M. Schulz (2001), Simulations of diffuse aurora with plasma sheet electrons in pitch angle diffusion less than everywhere strong, *J. Geophys. Res.*, *106*(A12), 28,949–28,966, doi:10.1029/2001JA000138.
Christon, S. P., D. J. Williams, D. G. Mitchell, L. A. Frank, and C. Y. Huang (1989), Spectral characteristics of plasma sheet ion and electron populations during undisturbed geomagnetic conditions, *J. Geophys. Res.*, *94*, 13,409–13,424, doi:10.1029/JA094iA10p13409.
Dubyagin, S., V. Sergeev, S. Apatenkov, V. Angelopoulos, A. Runov, R. Nakamura, W. Baumjohann, J. McFadden, and D. Larson (2011), Can flow bursts penetrate into the inner magnetosphere?, *Geophys. Res. Lett.*, *38*, L08102, doi:10.1029/2011GL047016.

Erickson, G. M., and R. A. Wolf (1980), Is steady convection possible in the Earth's magnetotail?, *Geophys. Res. Lett.*, *7*, 897–900, doi:10.1029/GL007i011p00897.

Erickson, G. M., R. W. Spiro, and R. A. Wolf (1991), The physics of the Harang discontinuity, *J. Geophys. Res.*, *96*, 1633–1645, doi:10.1029/90JA02344.

Gkioulidou, M., C.-P. Wang, L. R. Lyons, and R. A. Wolf (2009), Formation of the Harang reversal and its dependence on plasma sheet conditions: Rice convection model simulations, *J. Geophys. Res.*, *114*, A07204, doi:10.1029/2008JA013955.

Gkioulidou, M., C.-P. Wang, and L. R. Lyons (2011), Effect of self-consistent magnetic field on plasma sheet penetration to the inner magnetosphere: Rice convection model simulations combined with modified Dungey force-balanced magnetic field solver, *J. Geophys. Res.*, *116*, A12213, doi:10.1029/2011JA016810.

Gkioulidou, M., C.-P. Wang, S. Wing, L. R. Lyons, R. A. Wolf, and T.-S. Hsu (2012), Effect of an MLT dependent electron loss rate on the magnetosphere-ionosphere coupling, *J. Geophys. Res.*, *117*, A11218, doi:10.1029/2012JA018032.

Harang, L. (1946), The mean field of disturbance of polar geomagnetic storms, *Terr. Magn. Atmos. Electr.*, *51*, 353–380, doi:10.1029/TE051i003p00353.

Harel, M., R. A. Wolf, P. H. Reiff, R. W. Spiro, W. J. Burke, F. J. Rich, and M. Smiddy (1981), Quantitative simulation of a magnetospheric substorm 1. Model logic and overview, *J. Geophys. Res.*, *86*(A4), 2217–2241, doi:10.1029/JA086iA04p02217.

Hau, L.-N. (1991), Effects of steady state adiabatic convection on the configuration of the near-Earth plasma sheet, 2, *J. Geophys. Res.*, *96*(A4), 5591–5596, doi:10.1029/90JA02619.

Heppner, J. P. (1972), The Harang discontinuity in auroral belt ionospheric currents, *Geophys. Publ.*, *29*, 105.

Iijima, T., and T. A. Potemra (1976), The amplitude distribution of field-aligned currents at northern high latitudes observed by Triad, *J. Geophys. Res.*, *81*(13), 2165–2174, doi:10.1029/JA081i013p02165.

Jiang, F., M. G. Kivelson, R. J. Strangeway, K. K. Khurana, and R. Walker (2015), Ionospheric flow shear associated with the preexisting auroral arc: A statistical study from the FAST spacecraft data, *J. Geophys. Res. Space Physics*, *120*, 5194–5213, doi:10.1002/2013JA019255.

Kamide, Y., and S. Matsushita (1979), Simulation studies of ionospheric electric fields and currents in relation to field-aligned currents, 1. Quiet periods, *J. Geophys. Res.*, *84*(A8), 4083–4098, doi:10.1029/JA084iA08p04083.

Kaufmann, R. L., W. R. Paterson, and L. A. Frank (2004), Pressure, volume, density relationships in the plasma sheet, *J. Geophys. Res.*, *109*, A08204, doi:10.1029/2003JA010317.

Kim, H.-S., D.-Y. Lee, S. Ohtani, M.-Y. Park, and B.-H. Ahn (2012), On near-tail bubble penetration into geosynchronous altitude, *J. Geophys. Res.*, *117*, A07205, doi:10.1029/2012JA017749.

Kissinger, J., R. L. McPherron, T.-S. Hsu, and V. Angelopoulos (2012), Diversion of plasma due to high pressure in the inner magnetosphere during steady magnetospheric convection, *J. Geophys. Res.*, *117*, A05206, doi:10.1029/2012JA017579.

Kissinger, J., F. D. Wilder, R. L. McPherron, T.-S. Hsu, J. B. H. Baker, and L. Kepko (2013), Statistical occurrence and dynamics of the Harang discontinuity during steady magnetospheric convection, *J. Geophys. Res. Space Physics*, *118*, 5127–5135, doi:10.1002/jgra.50503.

Lemon, C., R. A. Wolf, T. W. Hill, S. Sazykin, R. W. Spiro, F. R. Toffoletto, J. Birn, and M. Hesse (2004), Magnetic storm ring current injection modeled with the Rice Convection Model and a self-consistent magnetic field, *Geophys. Res. Lett.*, *31*, L21801, doi:10.1029/2004GL020914.

Lessard, M. R., W. Lotko, J. LaBelle, W. Peria, C. W. Carlson, F. Creutzberg, and D. D. Wallis (2007), Ground and satellite observations of the evolution of growth phase auroral arcs, *J. Geophys. Res.*, *112*, A09304, doi:10.1029/2006JA011794.

Liu, W. W. (2006), Heat flux in magnetospheric convection: A calculation based on adiabatic drift theory, *Geophys. Res. Lett.*, *33*, L19104, doi:10.1029/2006GL027218.

Maynard, N. C. (1974), Electric field measurements across the Harang discontinuity, *J. Geophys. Res.*, *79*, 4620–4631, doi:10.1029/JA079i031p04620.

Motoba, T., K. Hosokawa, A. Kadokura, and N. Sato (2012), Magnetic conjugacy of northern and southern auroral beads, *Geophys. Res. Lett.*, *39*, L08108, doi:10.1029/2012GL051599.

Motoba, T., S. Ohtani, B. J. Anderson, H. Korth, D. G. Mitchell, L. J. Lanzerotti, K. Shiokawa, C. A. Kletzing, and G. D. Reeves (2015), On the formation and origin of substorm growth phase/onset auroral arcs inferred from conjugate space-ground observations, *J. Geophys. Res. Space Physics*, *120*, 8707–8722, doi:10.1002/2015JA021676.

Nielsen, N. E., and R. A. Greenwald (1979), Electron flow and visual aurora at the Harang discontinuity, *J. Geophys. Res.*, *84*, 4189–4200, doi:10.1029/JA084iA08p04189.

Nishimura, Y., L. R. Lyons, T. Kikuchi, V. Angelopoulos, E. F. Donovan, S. B. Mende, and H. Lühr (2012), Relation of substorm pre-onset arc to large-scale field-aligned current distribution, *Geophys. Res. Lett.*, *39*, L22101, doi:10.1029/2012GL053761.

Ohtani, S., H. J. Singer, and T. Mukai (2006), Effects of the fast plasma sheet flow on the geosynchronous magnetic configuration: Geotail and GOES coordinated study, *J. Geophys. Res.*, *111*, A01204, doi:10.1029/2005JA011383.

Ohtani, S., S. Wing, G. Ueno, and T. Higuchi (2009), Dependence of premidnight field-aligned currents and particle precipitation on solar illumination, *J. Geophys. Res.*, *114*, A12205, doi:10.1029/2009JA014115.

Ohtani, S., S. Wing, P. T. Newell, and T. Higuchi (2010), Locations of nightside precipitation boundaries relative to R2 and R1 currents, *J. Geophys. Res.*, *115*, A10233, doi:10.1029/2010JA015444.

Schulz, M., and M. Chen (2008), Field-line (Euler-potential) model of the ring current, 327, *J. Atmos. Sol. Terr. Phys.*, *70*, 482–489, doi:10.1016/j.jastp.2007.08.063.

Toffoletto, F., S. Sazykin, R. Spiro, and R. Wolf (2003), Inner magnetospheric modeling with the Rice Convection Model, *Space Sci. Rev.*, *107*, 175–196, doi:10.1023/A:1025532008047.

Vasyliunas, V. M. (1970), Mathematical models of magnetospheric convections and its coupling to the ionosphere, in *Particles and Fields in the Magnetosphere*, edited by B. M. McCormac, pp. 60–71, D. Reidel, Norwell, Mass.

Wang, C.-P., L. R. Lyons, M. W. Chen, and F. R. Toffoletto (2004), Modeling the transition of the inner plasma sheet from weak to enhanced convection, *J. Geophys. Res.*, *109*, A12202, doi:10.1029/2004JA010591.

Wang, C.-P., L. R. Lyons, R. A. Wolf, T. Nagai, J. M. Weygand, and A. T. Y. Lui (2009), Plasma sheet $PV^{5/3}$ and nV and associated plasma and energy transport for different convection strengths and *AE* levels, *J. Geophys. Res.*, *114*, A00D02, doi:10.1029/2008JA013849.

Weygand, J. M., R. L. McPherron, H. Frey, O. Amm, K. Kauristie, A. T. Viljanen, and A. Koistinen (2008), Relation of substorm onset to Harang discontinuity, *J. Geophys. Res.*, *113*, A04213, doi:10.1029/2007JA012537.

Wolf, R. A. (1983), The quasi–static (slow–flow) region of the magnetosphere, in *Solar Terrestrial Physics*, edited by R. L. Carovillano and J. M. Forbes, pp. 303–368, D. Reidel, Hingham, Mass.

Wolf, R. A., Y. Wan, X. Xing, J.-C. Zhang, and S. Sazykin (2009), Entropy and plasma sheet transport, *J. Geophys. Res.*, *114*, A00D05, doi:10.1029/2009JA014044.

Xing, X., and R. A. Wolf (2007), Criterion for interchange instability in a plasma connected to a conducting ionosphere, *J. Geophys. Res.*, *112*, A12209, doi:10.1029/2007JA012535.

Xing, X., L. R. Lyons, V. Angelopoulos, D. Larson, J. McFadden, C. Carlson, A. Runov, and U. Auster (2009), Azimuthal plasma pressure gradient in quiet time plasma sheet, *Geophys. Res. Lett.*, *36*, L14105, doi:10.1029/2009GL038881.

Yang, J., F. Toffoletto, G. Lu, and M. Wiltberger (2014), RCM-E and AMIE studies of the Harang reversal formation during a steady magnetospheric convection event, *J. Geophys. Res. Space Physics*, *119*, 7228–7242, doi:10.1002/2014JA020207.

Zou, S., L. R. Lyons, C.-P. Wang, A. Boudouridis, J. M. Ruohoniemi, P. C. Anderson, P. L. Dyson, and J. C. Devlin (2009a), On the coupling between the Harang reversal evolution and substorm dynamics: A synthesis of SuperDARN, DMSP, and IMAGE observations, *J. Geophys. Res.*, *114*, A01205, doi:10.1029/2008JA013449.

Zou, S., L. R. Lyons, M. J. Nicolls, C. J. Heinselman, and S. B. Mende (2009b), Nightside ionospheric electrodynamics associated with substorms: PFISR and THEMIS ASI observations, *J. Geophys. Res.*, *114*, A12301, doi:10.1029/2009JA014259.